

A TRMM-Based Tropical Cyclone Cloud and Precipitation Feature Database

HAIYAN JIANG

Department of Earth and Environment, Florida International University, Miami, Florida

CHUNTAO LIU AND EDWARD J. ZIPSER

Department of Atmospheric Sciences, University of Utah, Salt Lake City, Utah

(Manuscript received 24 September 2010, in final form 24 December 2010)

ABSTRACT

The Tropical Rainfall Measuring Mission (TRMM) satellite has provided invaluable data for tropical cyclone (TC) research since December 1997. The challenge, however, is how to analyze and efficiently utilize all of the information from several instruments on TRMM that observe the same target. In this study, a tropical cyclone precipitation, cloud, and convective cell feature (TCPF) database has been developed by using observations of the TRMM precipitation radar (PR), Microwave Imager (TMI), Visible and Infrared Scanner (VIRS), Lightning Imaging System (LIS), and the TRMM 3B42 rainfall product. The database is based on an event-based method that analyzes the measurements from multiple sensors. This method condenses the original information of pixel-level measurements into the properties of events, which can significantly increase the efficiency of searching and sorting the observed historical TCs. With both convective and rainfall properties included, the database offers the potential to aid the research aiming to improve both TC intensification and rainfall forecasts. Using the TRMM TCPF database, regional variations of TC convection and diurnal variations of TC rainfall are examined. In terms of absolute number, the northwest Pacific Ocean basin has the deepest and most intense T CPFs according to IR, radar, and 85-GHz microwave measurements. However, the North Atlantic T CPFs appear to have the highest lightning production. Globally, TC rainfall has a maximum at 0430–0730 local solar time (LST) and a minimum around 1930–2230 LST. However, after separating ocean from land, a distinct difference is seen. Over land, the diurnal variation of TC rainfall shows double peaks: one around 0130–0730 LST and the other at 1630–1930 LST. The minimum is at 1030–1330 LST.

1. Introduction

Tropical cyclones (TCs) are important producers of both cloud cover and precipitation in the tropics and subtropics. In TC research, there are two equally important areas that need more efforts: 1) how to improve the prediction of TC intensification and 2) how to improve the TC rainfall forecast. For TC intensification, especially rapid intensification (RI), one of the critical questions is what the necessary and sufficient conditions are. Favorable large-scale environmental conditions that are near-universally agreed to be necessary include warm sea surface temperature (SST), high low- to midlevel moisture, and low vertical wind shear (Gray 1968). Other factors such as

high ocean heat content (Shay et al. 2000), enhanced heat and moisture flux (Bosart et al. 2000), and whether a TC is well below its maximum potential intensity (Kaplan and DeMaria 2003) were also found to be related to RI. Defining sufficient conditions is still controversial, especially the possible role of intense convective events. Early studies suggested that hot towers (Simpson et al. 1998) and convective bursts (Steranka et al. 1986) near the eye are related to TC intensity change. Cecil and Zipser (1999) examined the relationships between TC intensity change and various convective parameters. They found that the strongest correlation involves the spatial coverage of at least moderate inner-core rainfall. Similarly, Kerns and Zipser (2009) found that enhanced TC genesis probability is associated with greater cold cloud area and raining area, especially in the eastern North Pacific Ocean. Using a limited subset of Tropical Rainfall Measuring Mission (TRMM) precipitation radar (PR) and Weather Surveillance Radar-1988 Doppler (WSR-88D) data, Kelley et al.

Corresponding author address: Dr. Haiyan Jiang, Department of Earth and Environment, Florida International University, 11200 SW 8th Street, PC-342B, Miami, FL 33199.
E-mail: haiyan.jiang@fiu.edu

(2004, 2005) found that the chance of TC intensification increases when one or more hot towers exist in the eye-wall. Yet uncertainties remain and additional quantification with a larger database is highly desirable.

In recent decades, freshwater flooding has become one of the main threats to human life when a TC makes landfall (Rappaport 2000). The rainfall climatology and persistence model (R-CLIPER; Tuleya et al. 2007) is one of the major tools used by the National Hurricane Center (NHC) for TC rainfall forecasts. The operational R-CLIPER uses radial distributions of azimuthally averaged TC rain rates derived from satellite to construct an instantaneous rainfall footprint as a function of storm intensity (Lonfat et al. 2007). The improvement of the statistical rainfall prediction technique relies heavily on satellite-based rainfall estimations and the regional climatology of TC rainfall.

TRMM (Kummerow et al. 1998) marks the first time that TCs in all ocean basins can be viewed by high-resolution down-looking precipitation radar. After 12 years of successful operation, TRMM measurements, along with numerical model-based reanalysis, have provided invaluable sources of TC data for the study of TC intensification, rainfall, and environment. On the TRMM satellite, PR can provide detailed vertical distribution of radar reflectivity. The TRMM Microwave Imager (TMI) can provide some information on vertically integrated ice and water path. The Visible and Infrared Scanner (VIRS) can provide information on cloud-top temperature and reflectance. At the same time, the Lightning Imaging Sensor (LIS) estimates lightning flash counts and rates. With several instruments observing the same target, how to analyze and efficiently utilize all this information was a scientific challenge.

The University of Utah (UU) TRMM Precipitation Feature (PF) database (<http://trmm.chpc.utah.edu/>) provides an excellent solution by using an event-based method to define PFs (Nesbitt et al. 2000). This method groups the spatially adjacent pixels with near-surface PR reflectivity greater than or equal to 20 dBZ or ice-scattering signature defined by TMI 85-GHz polarization corrected temperature (PCT; Spencer et al. 1989) less than or equal to 250 K. Liu et al. (2008) improved the database by using multiple definitions of cloud and precipitation features to increase its applicability to wider research areas. Besides a series of cloud and precipitation feature definitions summarized in Liu et al. (2008), convective cell features are recently added into version 6.2 of the database.

This paper introduces a TC subset of the UU TRMM PF database based on the collaboration between Florida International University (FIU) and UU. This FIU-UU TRMM TC precipitation, cloud, and convective cell feature (TCPF) database is constructed with TC features

identified from 12 years of TRMM observations by using TC best-track data (Landsea et al. 2004, 2008). The TRMM-based multisatellite 3B42 rainfall product (Huffman et al. 2007) provides a higher temporal resolution (3 hourly) and larger spatial coverage (50°S–50°N) for precipitation estimates than TRMM-only observations. The 3B42 product is based on two different sets of sensors: microwave and IR. Microwave data are collected by various low-orbit satellites, including TMI, the Special Sensor Microwave Imager (SSM/I), the Advanced Microwave Scanning Radiometer for the Earth Observing System (AMSR-E), and the Advanced Microwave Sounding Unit (AMSU). Precipitation estimates are derived from TMI, SSM/I, and AMSR-E microwave data by applying the Goddard profiling algorithm (GPROF; Kummerow et al. 1996). AMSU microwave measurements are converted to rainfall estimates by using the AMSU-B algorithm (Zhao and Weng 2002; Weng et al. 2003). IR data are collected by the international constellation of geosynchronous-earth-orbit (GEO) satellites. Here we also construct TRMM 3B42 TCPFs and non-TCPFs as a parallel product of the database. Then the populations and sizes of TCPFs, regional climatology of TC convection as derived from the PR vertical reflectivity structure and other TRMM sensors, and the diurnal cycle of TC rainfall are studied using the database.

2. Database development

Figure 1 shows the construction flowchart of the TRMM TCPF database with three levels of TRMM data processing. First, the global TC best-track data are collected and interpolated into TRMM observation times. Then TCPFs are identified if the distance between TC center and the TRMM PF center is less than 500 km. TCPFs and non-TCPFs are saved separately. Using the characteristics of identified features, global climatological descriptions of precipitation, cloud, and convective cell feature populations, occurrences, and other statistics are generated. The 3B42 TCPFs are generated in a similar way. This section introduces the methods used in generating three levels of TRMM and 3B42 TCPFs data.

a. Best-track data

Positions and maximum sustained surface winds of TCs are reported every 6 h as part of the best-track datasets. Six TC-prone basins are considered in this study: Atlantic (ATL), eastern + central Pacific (EPA), northwestern Pacific (NWP), northern Indian Ocean (NIO), southern Indian Ocean (SIO), and South Pacific (SPA). The best-track data of the ATL and EPA basins are obtained from NHC. For the other four basins, these data are from the U.S. Navy's Joint Typhoon Warning Center

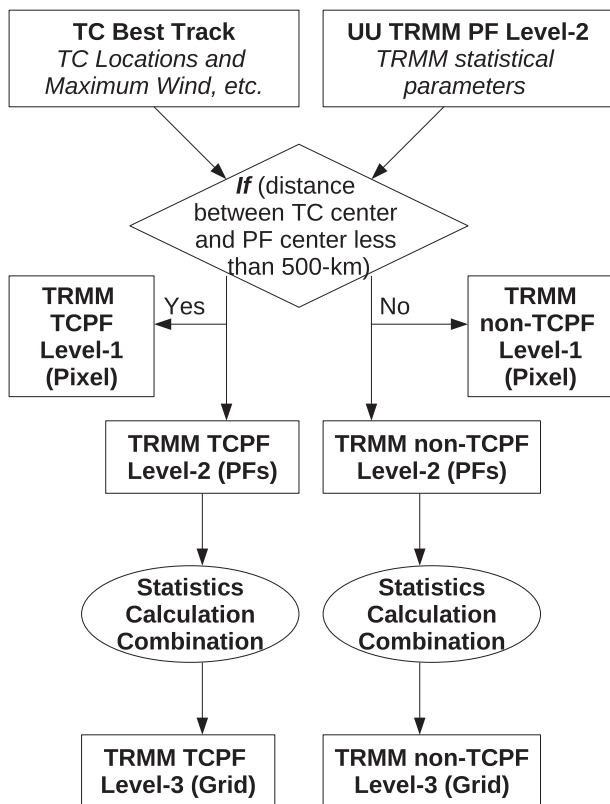


FIG. 1. FIU-UU TRMM TCPF database construction flowchart.

(JTWC). A total of 1022 storms that reached tropical storm intensity level or above are identified globally during 1998–2009 (Fig. 2). The JTWC best-track data do not provide TC names. We added this information by looking at the TC annual report from JTWC. Both NHC and JTWC best-track data do not record landfalling TCs formally. For example, NHC data only record U.S. hit cases, while JTWC best-track data have no information about whether a TC makes landfall. We carefully checked TC annual reports along with best-track images for all these storms and added a landfall flag in the best-track data. All mainland and small island landfalls are included. Table 1 lists numbers of TCs and landfalling TCs for each year and each basin. During the 12-yr period, globally 458 out of 1022 TCs made landfall. The highest fraction of landfalling TCs is seen in the NIO at 77%. The second and third highest fractions are in the ATL and NWP at 64% and 61%, respectively.

b. Generating TRMM TCPF level 1 and level 2 from the UU TRMM PF database

To find TRMM PFs that are related to TCs, best-track data are linearly interpolated into TRMM observation time of each feature with at least four PR pixels (one TMI pixel) for PR (TMI) swath features. If the distance

between PF center and TC center at the time of TRMM observation is less than 500 km, this PF is defined as a TCPF. Here the PF center is simply defined by the geographical center derived from averaging the minimum and maximum latitude and longitude of a PF. Previous TC rainfall studies used a 500-km (Lonfat et al. 2004), 550-km (Douglas and Englehart 2001), or 5° (Larson et al. 2005) radius as a threshold to define TC raining area. Douglas and Englehart (2001) found that in 90% of the cases the distance between the center of a storm and the outer edge of its cloud shield is less than 550–600 km. It is important to note that the definition used in this study is not a simple truncation at a 500-km radius. Instead, it includes cloud or precipitation areas beyond 500 km as long as the center of their parent PF is within 500 km of the TC center. Usually cloud or raining areas with a 600–750-km radius are included, but the definition does not include those isolated small features, which are not related to the storm. For users who are interested in the impact on rainfall of interactions between tropical cyclones and other weather systems, they can use the level 1 TCPF data described below that include a 20° longitude × 20° latitude TC centered box.

A series of storm parameters are calculated from the best-track information. These parameters include: land-ocean flag of TC center at the time of TRMM observation and 12- and 24-h future, storm 12-, 24-, 36-, and 48-h future intensity changes, storm direction, and speed of motion. All storm parameters are linearly interpolated into TRMM observation time from 6-hourly best-track data. These storm parameters—along with the statistical parameters from measurements and retrievals from PR, TMI, VIRS, and LIS in the UU TRMM PF level 2 data—are saved into the level 2 of TCPF data.

According to information obtained in the level 2 TCPF data, 13 677 individual TRMM TC overpasses are identified during 1998–2009 (Fig. 3). Because of the limited swath widths of TRMM TMI (760 km wide before the TRMM orbit boost during August 2001 and 878 km after the boost) and PR (215 km wide before boost and 247 km after boost), not all TRMM TC overpasses captured the storm in full. A TMI overpass is considered a good view if the distance between TC center and TMI swath center is less than 300 km. A PR overpass is considered a good view if the distance between TC center and PR swath center is less than 100 km. From Fig. 3, we can see that there are more than half of these TC orbits with a good view of the TC by the TMI swath. However, only 2315 of 13 677 overpasses have a good view of the TC by the PR swath. TRMM measurements from different instruments have been collocated and saved into level 1 (pixel level) of the UU TRMM PF data [see Liu et al. (2008) for the detailed collocation method and Liu (2007) for a list of parameters

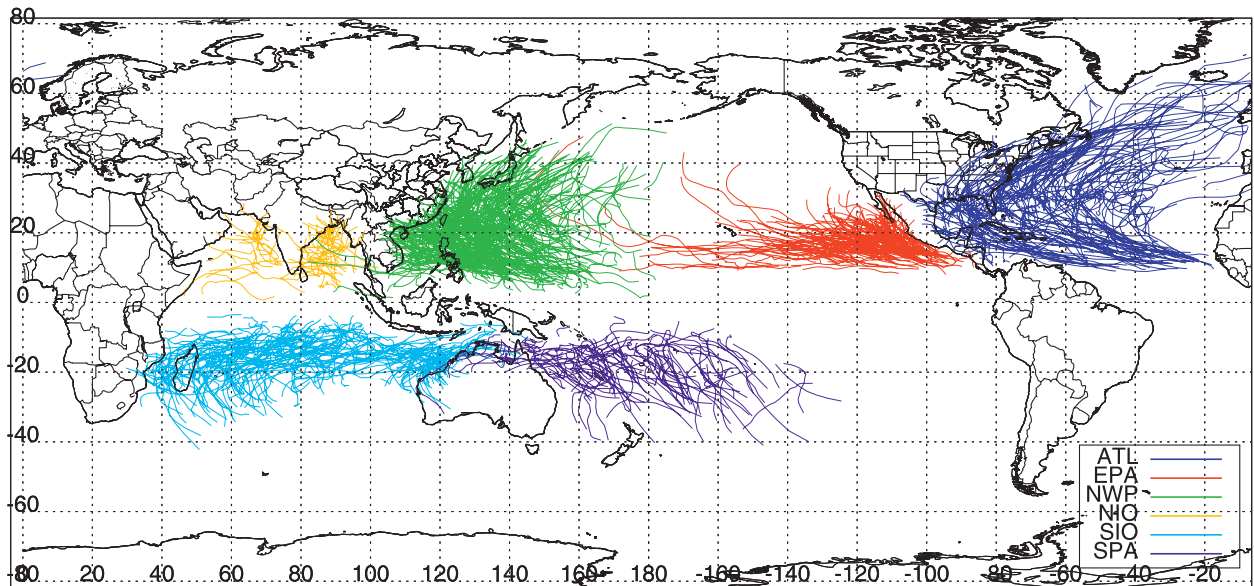


FIG. 2. Global TC best tracks in six basins during 1998–2009.

saved in level 1]. The collocated TRMM datasets include version 6 VIRS radiances (1B01), TMI brightness temperatures (1B11), rainfall retrievals from TMI (2A12; Kummerow et al. 2001), stratiform and convective rainfall categorizations (2A23; Steiner et al. 1995; Awaka

et al. 1998), rainfall retrieval from PR (2A25; Iguchi et al. 2000), and LIS flashes (<http://daac.gsfc.nasa.gov/data/datapool/TRMM/>). Here we generate the TC subset of level 1 data by cutting a 20° longitude \times 20° latitude TC centered box, which is typically large enough to

TABLE 1. Numbers of TCs and landfalling TCs for each year and each basin.

| | | ATL | EPA | NWP | NIO | SIO | SPA | Tot |
|-----------|------------------------------|-----|-----|-----|-----|-----|-----|------|
| 1998 | No. of TCs | 14 | 13 | 18 | 8 | 16 | 20 | 89 |
| | No. of landfall TCs | 9 | 2 | 14 | 6 | 7 | 2 | 40 |
| 1999 | No. of TCs | 12 | 9 | 23 | 5 | 20 | 12 | 81 |
| | No. of landfall TCs | 8 | 1 | 17 | 4 | 6 | 1 | 37 |
| 2000 | No. of TCs | 15 | 18 | 25 | 4 | 17 | 9 | 88 |
| | No. of landfall TCs | 11 | 2 | 12 | 3 | 5 | 3 | 36 |
| 2001 | No. of TCs | 15 | 15 | 29 | 3 | 14 | 7 | 83 |
| | No. of landfall TCs | 9 | 1 | 16 | 1 | 3 | 3 | 33 |
| 2002 | No. of TCs | 12 | 15 | 24 | 4 | 17 | 8 | 80 |
| | No. of landfall TCs | 9 | 2 | 14 | 3 | 6 | 1 | 35 |
| 2003 | No. of TCs | 16 | 16 | 23 | 3 | 18 | 10 | 86 |
| | No. of landfall TCs | 9 | 5 | 14 | 2 | 6 | 2 | 38 |
| 2004 | No. of TCs | 15 | 12 | 31 | 5 | 15 | 6 | 84 |
| | No. of landfall TCs | 9 | 1 | 16 | 4 | 4 | 2 | 36 |
| 2005 | No. of TCs | 28 | 15 | 24 | 6 | 18 | 8 | 99 |
| | No. of landfall TCs | 17 | 1 | 16 | 4 | 2 | 2 | 42 |
| 2006 | No. of TCs | 10 | 19 | 21 | 6 | 15 | 8 | 79 |
| | No. of landfall TCs | 8 | 3 | 15 | 4 | 5 | 2 | 37 |
| 2007 | No. of TCs | 15 | 11 | 22 | 6 | 14 | 9 | 77 |
| | No. of landfall TCs | 10 | 2 | 14 | 5 | 7 | 4 | 42 |
| 2008 | No. of TCs | 16 | 17 | 27 | 6 | 21 | 7 | 94 |
| | No. of landfall TCs | 10 | 4 | 17 | 6 | 8 | 2 | 47 |
| 2009 | No. of TCs | 9 | 18 | 23 | 6 | 18 | 9 | 83 |
| | No. of landfall TCs | 4 | 3 | 13 | 5 | 6 | 3 | 34 |
| 12-yr tot | No. of TCs | 177 | 178 | 290 | 61 | 203 | 113 | 1022 |
| | No. of landfall TCs | 113 | 27 | 178 | 47 | 66 | 27 | 458 |
| | Fraction of landfall TCs (%) | 64 | 15 | 61 | 77 | 33 | 24 | 45 |

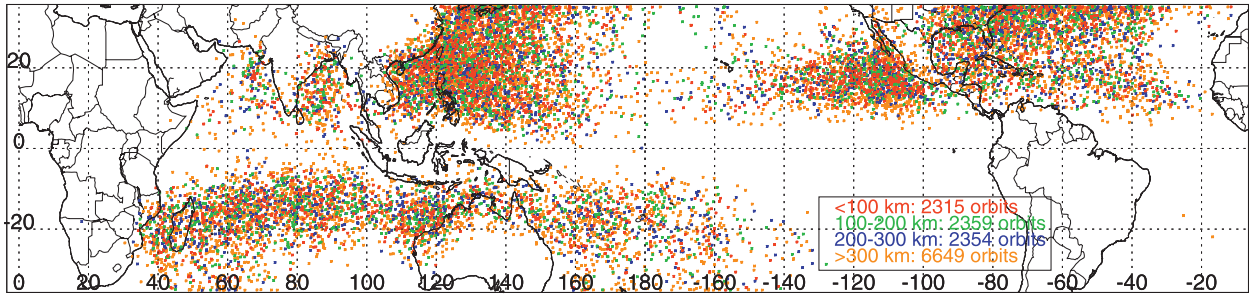


FIG. 3. Geographic distribution of TC observations from 1998 to 2009 in the FIU–UU TRMM TCPF database. Distances between TC center and the TRMM swath center are indicated in color.

observe the various sizes of TCs and their immediate environments.

Besides storm parameters, TRMM parameters in level 2 data structures are essentially the same as those in the UU TRMM PF level 2 as described in Liu et al. (2008), but with some new convective cell feature definitions added into the version 6.2 of TRMM PF database re-processing. Table 2 lists the definitions and criteria of 13 types of features included in the TRMM TCPF database. Some types of features are defined by using data only inside PR swath. Most of our feature definitions fall into this category. For inside PR swath definitions, features can be studied by using the collocated observations from PR, TMI, VIRS, and LIS. However, some feature

types are defined by using data inside TMI swath. Since TMI swath is wider, these definitions extend our capability to study larger storms (like TCs) by using TMI observations only. Definitions listed in Table 2 and summarized below are all for inside PR swath except otherwise indicated. There are five precipitation feature definitions: 1) radar precipitation feature (RPF) is defined by contiguous 2A25 near-surface raining pixels; 2) TMI precipitation feature in the PR swath (TPF) is defined by contiguous 2A12 surface raining pixels; 3) TMI precipitation feature in the TMI swath (TTPF) is defined by contiguous 2A12 surface raining pixels inside the TMI swath; 4) radar/TMI precipitation feature (RTPF) is defined by contiguous pixels with 2A25 near-surface or 2A12 surface rain greater

TABLE 2. Definition of precipitation, cloud, and convective cell features from 1998 to 2009 in the UU TRMM version-6.2 database. The features are all defined in PR swath if not indicated otherwise. The populations of total TRMM features and TC features are also listed.

| | Acronyms | Definitions | Criteria | Tot population | TCPF population |
|--------------------------|----------|--|--|----------------|-----------------|
| Precipitation features | RPF | Radar precipitation feature | Pixels with 2A25 rainfall rate $>0 \text{ mm h}^{-1}$ | 26 523 461 | 239 375 |
| | RPPF | Radar projection precipitation feature | Pixels with reflectivity $\geq 20 \text{ dBZ}$ anywhere above ground | 25 703 571 | 153 096 |
| | RTPF | Radar/TMI precipitation feature | Pixels with 2A25 or 2A12 rainfall rate >0 | 24 447 777 | 152 792 |
| | TPF | TMI precipitation feature | Pixels with 2A12 rainfall rate $>0 \text{ mm h}^{-1}$ | 13 286 077 | 97 246 |
| | TTPF | TMI precipitation feature in TMI swath | As above, but in TMI swath | 13 649 884 | 95 956 |
| Cold PCT features | TPCTF | TMI cold 85-GHz PCT feature with 250 K in TMI swath | Pixels with 85-GHz PCT $\leq 250 \text{ K}$ | 5 475 411 | 70 703 |
| | T200F | TMI cold 85-GHz PCT feature with 200 K in TMI swath | Pixels with 85-GHz PCT $\leq 200 \text{ K}$ | 1 303 750 | 18 539 |
| Cold cloud features | C210F | Cloud feature with 210 K | VIRS $T_{B11} \leq 210 \text{ K}$ | 1 529 363 | 39 962 |
| | C235F | Cloud feature with 235 K | VIRS $T_{B11} \leq 235 \text{ K}$ | 9 071 722 | 87 442 |
| Convective cell features | CLCONV | 2A23 convective cell feature | 2A23 convective pixels | 15 010 443 | 211 214 |
| | CL40P | Convective cell feature with radar projection reflectivity $>40 \text{ dBZ}$ | Pixels with reflectivity $\geq 40 \text{ dBZ}$ anywhere above ground | 2 694 447 | 62 653 |
| | CL6KM30 | Convective cell feature with 6 km $>30 \text{ dBZ}$ | Pixels with 6-km reflectivity $\geq 30 \text{ dBZ}$ | 1 354 985 | 33 188 |
| | CL12KM20 | Convective cell feature with 12 km $>20 \text{ dBZ}$ | Pixels with 12-km reflectivity $\geq 20 \text{ dBZ}$ | 352 581 | 6437 |

than zero; 5) radar projection precipitation feature (RPPF) is defined by grouping the area of ground projection of radar reflectivity greater than 20 dBZ, which includes thick anvils aloft. There are two cold PCT feature definitions (TPCTF and T200F), which are defined by pixels with 85-GHz PCT ≤ 250 and 200 K, respectively, in the TMI swath. Two types of cold cloud features are defined by using VIRS 10.8- μm brightness temperature $T_{\text{B11}} \leq 210$ (C210F) and 235 K (C235F). Convective cell feature definitions are introduced in order to better study the individual cells embedded in a large precipitation feature. Four types of cell features are defined by using 2A23 convective pixels (CLCONVF), radar projection reflectivity greater than or equal to 40 dBZ (CL40PF), PR 6-km reflectivity greater than or equal to 30 dBZ (CL6KM30F), and PR 12-km reflectivity greater than or equal to 20 dBZ (CL12KM20F).

Major parameters stored in level 2 data include those from PR algorithms 2A25 and 2A23, TMI algorithms 1B11 and 2A12, VIRS algorithm 1B01, LIS flash observations, and National Centers for Environmental Prediction (NCEP) reanalysis. Besides those parameters listed in Liu et al. (2008) and Liu (2007), the vertical profiles of 25-, 30-, 35-, 40-, 45-, and 50-dBZ area with 1-km vertical resolution, and areas of 37-GHz PCT < 275 , 250, 225, 200, and 175 K are also saved.

Figure 4 presents an example of feature definitions for Typhoon Mitag (2007) in the NWP basin and some parameters in the defined RPPF. In this case, the inside PR swath definitions (Figs. 4a,b,e-h) capture the strong convective core of the eyewall but miss a large raining region in the northwest quadrant. This is due to the truncation effect of the narrow PR swath (Nesbitt et al. 2006). In contrast, inside TMI swath definitions (Figs. 4c,d) capture almost the whole TC feature with minimal swath truncation effect in the 2A12 rain (Fig. 4c). Also there were large areas of thick anvil and cold clouds (Fig. 4e) in the southwestern quadrant of the storm without a strong ice-scattering signal (Fig. 4d) and hardly any surface rain (Figs. 4a,c). The TMI is a passive microwave radiometer with 10-, 19-, 22-, 37-, and 85-GHz channels. The 85- and 37-GHz channels can only detect the scattering signature from ice particles with diameters greater than about 0.1 mm. The TMI usually cannot observe signals from anvil clouds because ice particles in anvils are usually smaller than 0.1 mm. However, the VIRS 10.8- μm channel is sensitive to the cloud-top temperature. Therefore only cold cloud features defined by C210F and C235F can describe anvil clouds (Fig. 4e). The detailed vertical distributions of maximum reflectivity and 20- and 40-dBZ area can be summarized in RPPFs (Figs. 4b,i) and CL40PFs (Fig. 4b). The statistics of convective cells can be summarized in CLCONVFs (Fig. 4f), CL40PFs (Fig. 4b), CL6KM30Fs

(Fig. 4g), and CL12KM20Fs (Fig. 4h). The TC system can be described comprehensively with these multiple feature definitions. For example, several small convective cells are identified by cell feature definitions, and the contribution of these cells to total rain can be easily derived; the differences between 2A25 and 2A12 volumetric rain may be used to validate the performance of rain retrieval algorithms in TCs, and so on.

c. Generating 3B42 TCPF level 1 and level 2

Although in lower spatial resolution ($0.25^\circ \times 0.25^\circ$), the benefits of using the TRMM-based 3-hourly multisatellite rainfall product 3B42 are twofold: 1) higher temporal resolution and 2) larger spatial coverage (50°S – 50°N) to cover the whole lifetime of any TC. A TC subset of 3B42 rainfall data is constructed to supplement the TRMM TCPF data. Figure 5 shows the construction flowchart of the 3B42 TCPF database. Similar to the TRMM TCPF database, three levels of data are generated. However, unlike TRMM processing in which features are grouped first and then TCPFs are defined according to the distance from TC center, the first step is that all 3B42 raining pixels within a 500-km radius of the TC center are attributed to TC-related pixels and saved in level 1 TCPF data files. Other raining pixels are saved into level 1 non-TCPF data files. Then raining pixels are grouped for TC pixels and non-TC pixels separately. Storm best-track parameters as listed in section 2b and 3B42 rainfall parameters such as total volumetric rain, raining area, greater than 5 mm h^{-1} volumetric rain, and greater than 5 mm h^{-1} raining area are saved in level 2 files. TC pixels are identified before grouping to ensure that only TC-related raining pixels are included in the 3B42 TCPF data. Jiang and Zipser (2010) used two definitions of 3B42 TCPFs: the first one was the same as the one used here, while the second definition was to group raining pixels first and then attribute those PFs with center within 500-km radius of TC center as TCPFs. They found out that the second definition overestimates TC monthly rain by 1.5–3 times compared with the former 3B42 definition and 2A25 and 2A12 estimates. This is because, without the pixel-level 500-km restriction, sometimes a 3B42 TCPF could become very large and connected with other non-TC features. The reasons are 1) 3B42 features are relatively large in size because of the lower spatial resolution of the gridded 3B42 product, and 2) 3B42 sometime slightly overestimates rain rate from no-rain regions because of the combination of its low spatial resolution caused by microwave data and overestimation of rain in cold cloud regions caused by IR observations. By applying the pixel-level 500-km restriction first, it is guaranteed that only TC-related rainfall is included.

Figure 6 shows an example of the 3B42 TCPF definition and level 2 parameters for Hurricane Bonnie [1998;

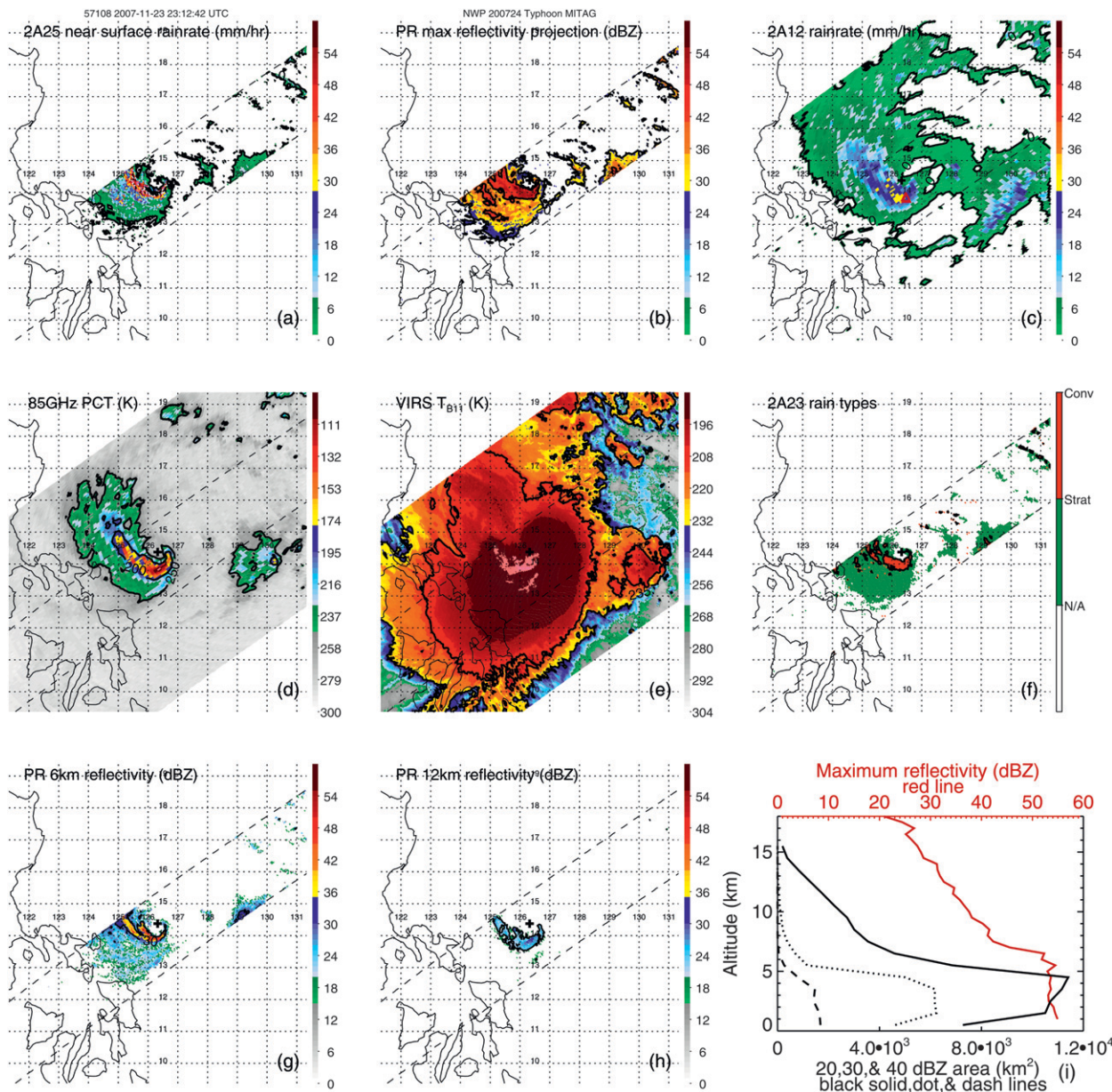


FIG. 4. Demonstration of the TCPF feature types using the case of Typhoon Mitag (2007). (a) 2A25 near-surface rain rate. RPF is defined by the area with rain shown by black contour. (b) The PR maximum-reflectivity ground projection. RPPF (CL40PF) is defined by area with 20 dBZ (40 dBZ) shown by black contours. (c) 2A12 surface rainfall rate. TTPF (TPF) is defined by area with rain shown by black contour in TMI (PR) swath. Red triangles are the location of flashes detected by LIS (note that there are two flashes in the same location; also see Table 2). (d) TMI 85-GHz PCT. TPCTF (T200F) is shown by 250-K (200 K) contour line. (e) VIRS T_{B11} C210F and C235F are defined by area with $T_{B11} < 210$ and 235 K shown by black contours inside the PR swath. (f) 2A23 rain types. CLCONVF is defined by area with spatially adjacent convective pixels shown by black contours. (g) The PR 6-km reflectivity. CL6KM30F is defined by the area with 30 dBZ at 6 km as shown by black contour. (h) The PR 12-km reflectivity. CL12KM20F is defined by the area with 20 dBZ at 12 km as shown by black contour. (i) Vertical profiles of 20-, 30-, and 40-dBZ area (black solid, dotted, and dashed lines, respectively) and the maximum reflectivity (red line) of the large RPPF defined in (b). The plus sign at the center of (a)–(h) is the typhoon center location. The dashed line in (a)–(h) is the edge of the PR swath. Note that there could be a truncation effect due to the narrow swath in defining large features (Nesbitt et al. 2006).

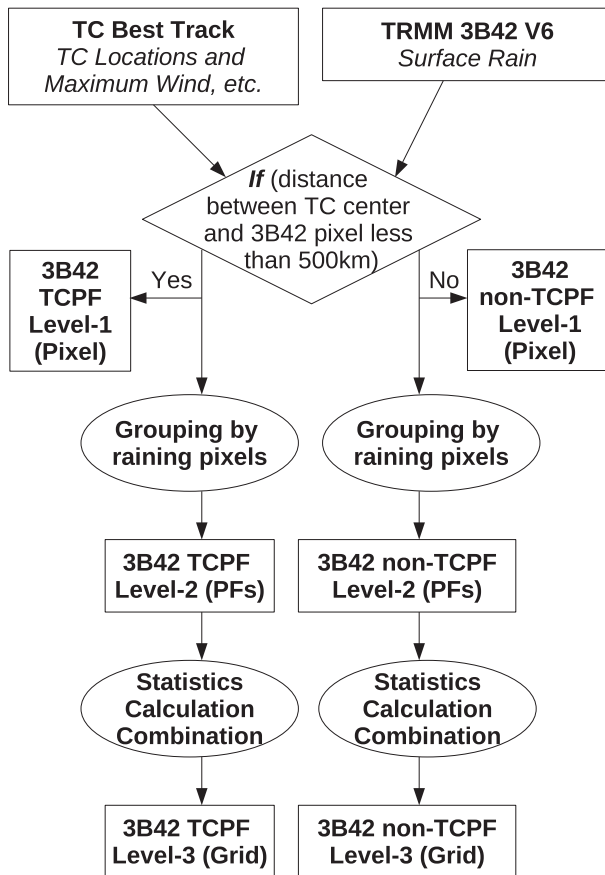


FIG. 5. FIU-UU TRMM 3B42 TCPF database construction flowchart.

the same case shown in Jiang and Zipser's (2010) Fig. 4]. Figure 6a presents how the TC raining area is connected with another feature because of the inability of 3B42 to identify nonraining regions between them. Using the 500-km pixel-level restriction eliminates the contamination. The lifetime rain accumulation of Bonnie (Fig. 6b) is derived from the level 1 3B42 TCPF data. Volumetric rain and raining area for all raining regions and heavy rain regions only (rain rate greater than 5 mm h^{-1}) can be summarized in level 2 (Figs. 6c,d). Table 3 lists some level 2 parameters of the 3B42 TCPF defined in Fig. 6a and the lifetime averages of these parameters for Bonnie. It is useful to evaluate the contribution of heavy rain regions to the total TC rain. From both Table 3 and Figs. 6c,d, we can see that the heavy rain regions only contribute to about 10%–20% of total raining area but contribute more than 50%–60% of total volumetric rain.

d. Generating TRMM and 3B42 TCPF level 3

To conveniently study the climatological characteristics of TCs, level 3 data are generated by summarizing statistics of feature properties onto a $1^\circ \times 1^\circ$ grid. Because

TRMM observations and 3B42 product include diurnal variations of properties of cloud and precipitation systems, they are categorized into eight local time periods.

Figure 7 demonstrates the mean TC monthly rain from level 3 of RPF, TTPF, and 3B42 TCPF data from 1998 to 2009. Climatological differences of TC rainfall for different basins can be examined from level 3 data. Also the differences among 2A25, 2A12, and 3B42 rain estimates for TC can be compared in a long-term basis. As noted by Liu et al. (2008), when we accumulate the volumetric rain from features onto grids, volumetric rain and raining area inside each feature are assigned to the grid where the mass-weighted centroid of that feature is located. This could be problematic when we assign volumetric rain and raining area from large cloud and precipitation features to a small grid (edge effect). To evaluate this problem for TCPFs, Fig. 7d shows the TC monthly rainfall calculated by counting the raining pixels inside the 3B42 grids, while Fig. 7c shows the TC monthly rainfall calculated by accumulating rain volume of PFs centered inside the grids. Their general patterns are very close, which demonstrates that the problem is minimized by the large sample size. However, since the size of 3B42 TCPFs is usually larger than that of TRMM-based TCPFs, the edge effect from TRMM TCPFs should be even smaller.

TCPFs and non-TCPFs are processed into separate level 3 data files. Table 4 lists the parameters in level 3. There are three types of parameters in level 3 data: 1) rain parameters, 2) population and total area parameters, and 3) maximum and minimum parameters. The last two types of parameters are basically convective proxies. All parameters are on $1^\circ \times 1^\circ$ grids for eight local time periods (0–3, 3–6, 6–9, . . . , 21–24 h). Level 3 products are processed for monthly, yearly, TC seasonal only (see Jiang and Zipser 2010 for details), and 12-yr (1998–2009) periods.

e. Web application

For both TC scientists and the general public, how to quickly search past storms observed by TRMM and get the data is an issue. Along with this study, we offer a Web application for users to easily find TRMM observations for each TC from December 1997 to December 2009 (<http://trmm.chpc.utah.edu/cyclone>). Currently the Web page is located in the UU TRMM data Web server domain, but it will be migrated to FIU soon. Numbers of storms and TRMM orbits are listed in a table by each year and each basin. A series of top-down Web pages allow users to click the year and basin of interest, then a storm of interest in the year and the basin. For each storm, the 3B42 rainfall accumulation image overlaid with best track and a list of TRMM orbits of the storm are accessible. After clicking the orbit of interest, users will be

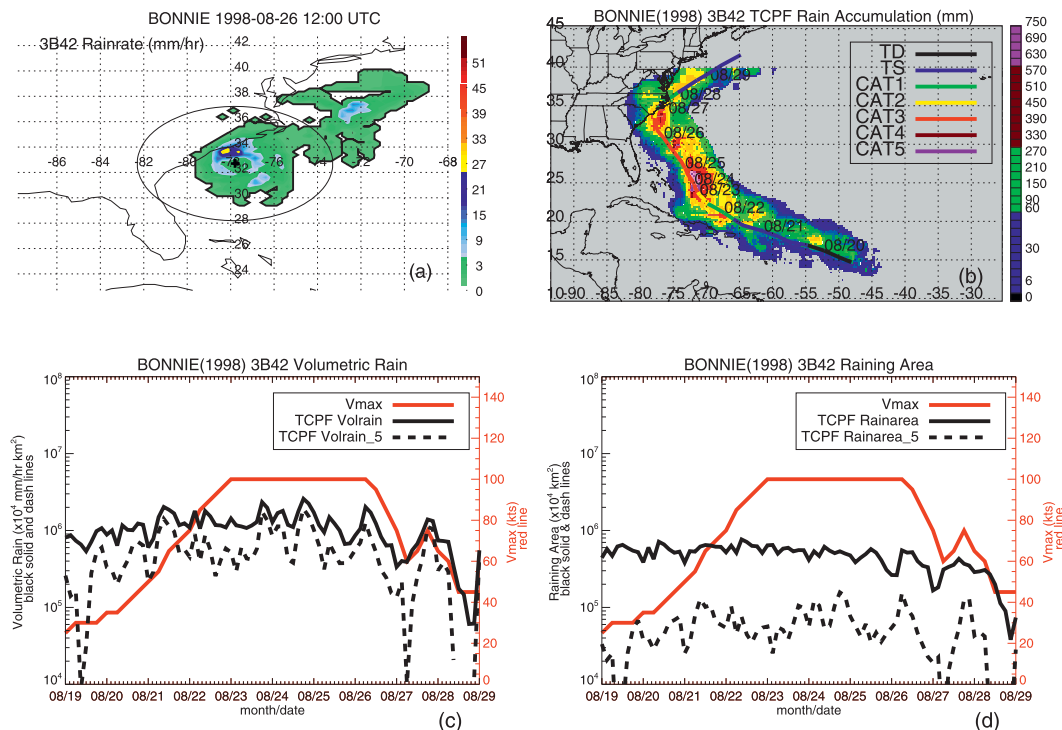


FIG. 6. Demonstration of 3B42 TCPF feature and parameters using the case of Hurricane Bonnie (1998). (a) 3B42 rain rate at 1200 UTC 26 Aug 1998. 3B42 TCPF feature is defined by the area both with rain rate $>0 \text{ mm h}^{-1}$ (black contour) and within the 500-km radius circle around the hurricane center. (b) Lifetime total rain accumulation from 3B42. (c) Time series of 3B42 TCPF volumetric rain for all rain regions and heavy rain regions (rain rate $> 5 \text{ mm h}^{-1}$). (d) Time series of 3B42 TCPF raining area for all rain regions and heavy rain regions (rain rate $> 5 \text{ mm h}^{-1}$). The 500-km radius circle around the storm center is indicated in (a). Bonnie’s best track is indicated in (b). The time series of Bonnie’s maximum surface wind speed is indicated in (c) and (d).

able to view the nine-panel TRMM image including PR near-surface reflectivity, PR maximum-reflectivity projection, 2A25 near-surface rain, 85-GHz PCT, 37-GHz PCT, 2A12 surface rain, VIRS T_{B11} , 2A23 rain types, and 2A23 storm height parameters plotted from the collocated level 1 data. TRMM TCPF level 1 data for each orbit and best-track data for each TC are downloadable. The Web page provides the TC center location, its distance to TRMM swath center, and best-track maximum wind for each orbit. Another interesting feature adapted from the UU TRMM data Web application is that the TRMM orbital data can be viewed and manipulated from a Google Earth background to produce both horizontal

images and PR vertical cross sections. For storms missed by TRMM (only 9 out of 1013 TCs during the period), only 3B42 rainfall accumulation images overlaid with best tracks are provided.

3. Research applications

a. Global distribution of TC convection

One important application of the TRMM TCPF database is to study the global distribution of TC convection. Cloud-top brightness temperatures from TRMM VIRS can be used to show how deep the convection is and how

TABLE 3. Some parameters of the 3B42 TCPF defined in Fig. 6a and the lifetime averages of these parameters for Bonnie.

| | Raining area (km ²) | Heavy raining area (for rain rate $>5 \text{ mm h}^{-1}$) (km ²) | Fraction of heavy raining area (%) | Rain vol (mm h ⁻¹ km ²) | Heavy rain vol (for rain rate $>5 \text{ mm h}^{-1}$) (mm h ⁻¹ km ²) | Fraction of heavy rain vol (%) |
|-----------------------------|---------------------------------|---|------------------------------------|--|--|--------------------------------|
| TCPF in Fig. 6a | 256 929 | 54 380 | 21 | 861 575 | 558 079 | 65 |
| Lifetime average for Bonnie | 401 266 | 47 586 | 12 | 938 202 | 467 634 | 50 |

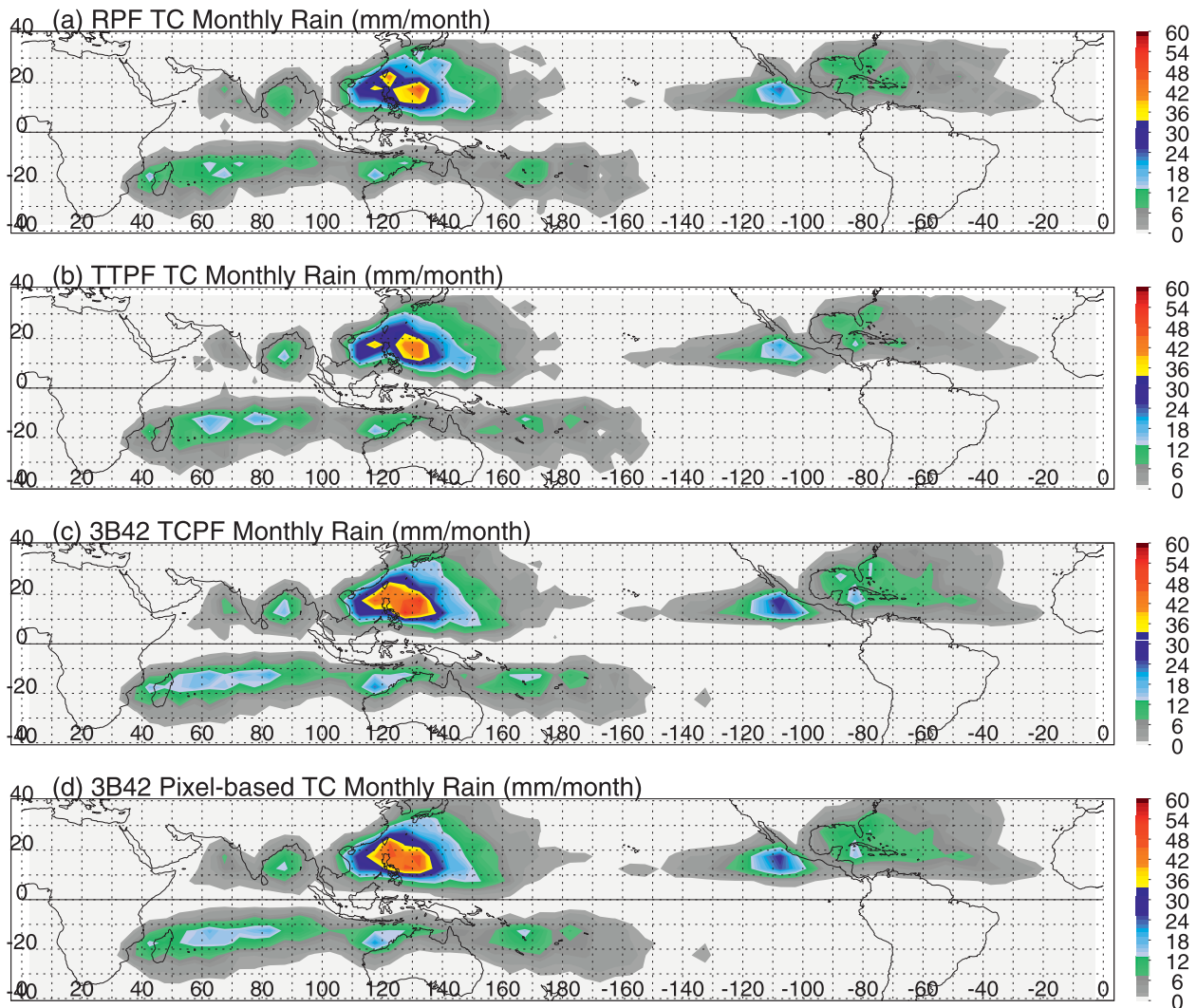


FIG. 7. (a) Mean 2A25 TC monthly rain from RPFs from 1998 to 2009. (b) Mean 2A12 TC monthly rain from TTPFs from 1998 to 2009. (c) Mean 3B42 TC monthly rain from 3B42 TCPFs from 1998 to 2009. (d) Mean 3B42 TC monthly rain from 3B42 TCPF level-1 raining pixels from 1998 to 2009.

cold the cloud tops are (Mapes and Houze 1993; Gettelman et al. 2002). To estimate the convective intensity, we adopt proxies that can be measured by the TRMM PR, TMI, and LIS (Mohr and Zipser 1996; Cecil and Zipser 2002; Zipser et al. 2006). Here three such parameters are used: minimum 85-GHz PCT measured by TMI, maximum 20-dBZ echo height measured by PR, and total flash count measured by LIS. To demonstrate the size of deep and/or intense convection, an area of minimum $T_{B11} \leq 210$ K, an area of minimum 85-GHz PCT < 250 K, and an area of 20 dBZ reaching 6 km are examined. Figure 8 presents locations and rareness of TCPFs according to these parameters for TC RPPFs from 1998 to 2009. For example, of the approximately 153 000 TCPFs, only about 10% have 20-dBZ echo higher than 8.5 km and 1% higher

than 15.25 km, and only about 1%–2% have lightning flash count greater than 1 flash per minute and 0.1% greater than 40 flashes per minute,¹ and so on. The deepest and most intense convection in TCs is distributed differently as defined by each proxy. The coldest IR cloud-top events (Fig. 8a) and tallest radar 20-dBZ echoes (Fig. 8b) are found mainly in the NWP, SIO, SPA, and NIO basins, while the most intense ice-scattering signature events indicated by minimum 85-GHz PCT (Fig. 8c) and extreme lightning events (Fig. 8d) are found more frequently in

¹ LIS's view time is 80 s for one location, which means the minimum detectable signal of 0.7 flashes per minute. The detection efficiency is estimated to be about 85% (Boccippio et al. 2002).

TABLE 4. List of parameters in level-3 TCPF data. All parameters are on $1^\circ \times 1^\circ$ grids for eight local time periods (0–3, 3–6, 6–9, . . . , 21–24 h).

| | |
|--------------------------------------|--|
| Rain parameters | 2A25, 2A12, and 3B42 rain vol 2A25, 2A12, and 3B42 raining area 2A25 convective and stratiform rain vol 2A25 convective and stratiform raining area 3B42 rain vol for heavy rain regions (rain rate > 5 mm h ⁻¹) 3B42 raining area for heavy rain regions (rain rate > 5 mm h ⁻¹) |
| Population and total area parameters | Total flash counts Total area of $T_{B11} < 210$, and 235 K Total area of 85-GHz PCT < 250, 200, 150, and 100 K Total area of 37-GHz PCT < 275, 250, 225, 200, and 175 K Total 20-, 25-, 30-, 40-, 45-, and 50-dBZ area at different alt |
| Max or min parameters | Max 20-, 30-, and 40-dBZ echo tops Max flash counts Max reflectivity at different altitudes Min T_{B11} Min 37- and 85-GHz PCT |

the NWP, ATL, and SIO than in the NIO, SPA, and EPA. As for area of deep/intense convection, the largest area events are concentrated over the NWP. It is not surprising that the coldest, most intense, and largest TC convection events are located in the western Pacific warm pool region. Previous studies using IR as primary data source often find that the tropical western Pacific Ocean has the greatest concentration of cold, high clouds (Gettelman et al. 2002). Although studies using TRMM PR and TMI often find that convective intensity is much stronger over land than over ocean (Liu and Zipser 2005; Zipser et al. 2006), for TCs that mainly occur over ocean, the NWP is more favorable than other basins. The large-scale environmental factors in the NWP that are favorable for TC and convection development include high SST, low wind shear (Gray 1968), high CAPE, and high neutral buoyancy level (Liu et al. 2007).

An interesting result demonstrated in Fig. 8 is the distinct contrast between the EPA and NWP. As seen for all parameters being examined here, the NWP has a high concentration of deepest and most intense TC convection, but the EPA has a relatively low concentration of that. This seems paradoxical because the highest TC number density regions are in both the NWP and EPA as shown in Jiang and Zipser’s (2010) Fig. 8. However, the highest TC number density does not necessarily mean the strongest TC convection. Also the western Pacific warm pool in the NWP is more favorable for deep convection than open ocean regions in the EPA.

There is a strong preference for extreme TC lightning events to be located over land or coastal regions, such as the southeastern coast of Asia, the eastern coast of Mexico and the United States, the Caribbean Islands, the western coast of Australia, the Baja California coast, and Madagascar (Fig. 8d). The distinct difference between land and

ocean for lightning occurrence has been found in previous studies for general convection (not limited to TCs) globally (Orville and Henderson 1986), within the tropics (Zipser 1994; Petersen and Rutledge 2001; Zipser et al. 2006), and for thunder clouds in Asian monsoon (Xu et al. 2010).

Another interesting result from Fig. 8 is that the ATL basin has a high concentration of most intense convection as defined by microwave ice-scattering signature (minimum 85-GHz PCT, Fig. 8c) and lightning (Fig. 8d) but a rather low concentration of coldest and tallest convection as seen from minimum T_{B11} (Fig. 8a) and maximum 20-dBZ echo height (Fig. 8b). Both the number of TC RPPFs with lightning and the total flash counts in TC RPPFs are higher in the ATL than all other basins (Table 5), with the NWP the second highest. However, the NWP has more total number of TC RPPFs, which makes the NWP the third highest in the population percentage of TC RPPFs with lightning, following the ATL and NIO. After normalizing the flash counts by sample size (total 2A25 raining area) of each basin (the fourth column of Table 5), lightning production in the ATL is the highest, and the SPA is the lowest. However, in all basins, TC lightning production is rather low, 1–4 flashes per 10⁴ square kilometer raining area. Black and Hallett (1986, 1999) note that it is rare to find updrafts in hurricanes that are strong enough to produce significant supercooled water and large graupel, and therefore significant charge separation (Takahashi 1978). Using 1-yr TRMM LIS observations, Cecil et al. (2002) found that tropical cyclones produce much less lightning than tropical continental precipitation systems. Because only fairly intense convection makes a significant contribution to lightning production, additional parameters for normalizing the flash counts are presented in Table 5. The last three columns in Table 5 make use of parameters to isolate more intense

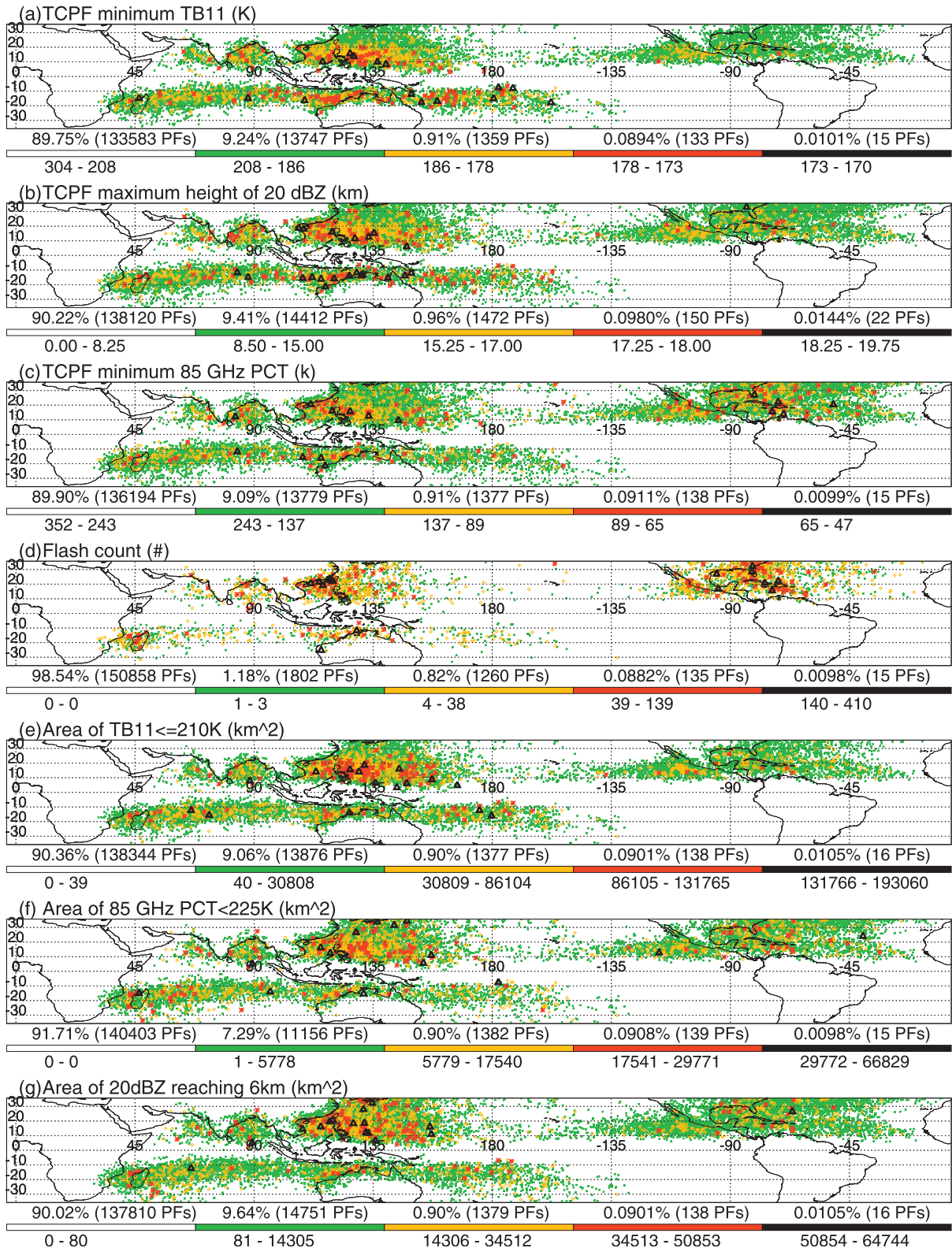


FIG. 8. Locations of deep convection events in TCs categorized by (a) minimum T_{B11} , (b) maximum height of 20-dBZ echo, (c) minimum 85-GHz PCT, (d) flash count, (e) area of $T_{B11} \leq 210$, (f) area of 85-GHz PCT < 250 K, and (g) area of 20 dBZ reaching 6 km. Rarity of the events is represented with green dot (approximately top 2% for flash count and approximately top 10% for all other parameters), orange dot (approximately top 1%), red star (approximately top 0.1%), and black triangle (approximately top 0.01%) symbols from TC RPPFs from 1998 to 2009.

TABLE 5. Number and percentage of TC RPPFs with lightning and lightning flash counts for each basin and ratios of flash count to various aspects of sample size. Units for flash count area columns are number per 10^4 square kilometers.

| Basin | No. of TC RPPFs with lightning | Population percentage of TC RPPFs with lightning | Flash count | Flash count per 2A25 raining area | Flash count per 2A23 convective certain area | Flash count per 85-GHz PCT <225 K area | Flash count per 8-km 35-dBZ area |
|-------|--------------------------------|--|-------------|-----------------------------------|--|--|----------------------------------|
| ATL | 1148 | 3.25 | 10 855 | 4.5 | 23.5 | 36.6 | 5966 |
| EPA | 246 | 1.48 | 1794 | 3.0 | 17.7 | 24.9 | 4454 |
| NWP | 966 | 2.07 | 9491 | 2.5 | 15.3 | 22.5 | 4269 |
| NIO | 182 | 2.83 | 1723 | 2.5 | 14.9 | 20.2 | 4115 |
| SIO | 470 | 1.44 | 3709 | 2.4 | 14.8 | 17.5 | 2981 |
| SPA | 161 | 1.31 | 881 | 1.2 | 8.1 | 11.1 | 3202 |

portions of TC convection. The convective certain area is defined by the total area of data points classified as “convective certain” by the TRMM PR 2A23 algorithm. Many previous studies (Mohr and Zipser 1996; Nesbitt and Zipser 2003) used 225 K of TMI measured 85-GHz PCT as a convection criterion in mesoscale convective systems (MCSs). Xu et al. (2010) found that 35-dBZ area at 8–9 km is best correlated with lightning production. Lightning production of TCs is 2–4 times greater in the ATL than SPA, and about 50% greater than the other four basins. Notice that the ATL basin domain includes many islands, which might be the contributor for higher lightning production. It is also possible that updrafts in TC convection in the ATL are more intense, but the level of neutral buoyancy and the height of the tropopause are climatologically lower in the ATL, which limits the maximum height that clouds can reach. A further study is needed to verify this.

Because small PFs are so numerous in comparison with large PFs, it is misleading to include the entire PF database for many important parameters. Therefore, Fig. 9 includes only those features that meet the MCS² definition as follows: TC RPPFs with areas greater than or equal to 1000 km² and containing at least one convective pixel (85-GHz PCT < 225 K). In the cumulative frequency distributions of minimum T_{B11} and maximum 20-dBZ height (Figs. 9a,b), the ATL TC RPPFs appear to produce low cloud top more often than TC RPPFs in other basins, consistent with what is seen in Figs. 8a,b. TC RPPFs in the SPA, NWP, and NIO have higher percentage of features with colder/taller cloud top, while those in EPA are somewhere in between. The NIO TC RPPFs are found to produce moderate to intense convection (maximum 20-dBZ height between 10 and 16 km, minimum 85-GHz PCT between 190 and 100 K, Figs. 9b,c) more often than those in other basins. This is mainly due to

the relative lack of small features with high minimum brightness temperatures and low maximum 20-dBZ echo height. Laing and Fritsch (1997) noted that there is a concentration of mesoscale convective complexes (MCCs) over the Indian subcontinent because of elevated terrain and prevailing midlevel flow. This special environment makes the NIO a unique TC-prone basin. Although the number of TCs is the lowest in this basin, convection associated with TCs in the NIO seems stronger than that in other basins. The cumulative distributions of sizes of TC convection are shown in Figs. 9d–f. The NWP (ATL) TC RPPFs appear to produce large convective features more (less) often than other basins; however, the differences among six basins are not big in all the cumulative distributions shown in Fig. 9.

b. Regional variations of vertical structure of radar echoes

Another application of the TRMM TCPF database is to study the regional variations of vertical structures of TCPFs. Figure 10 shows the 20-dBZ echo occurrence (area percentage). This parameter is calculated by using the 20-dBZ area inside TC RPPFs at selected heights divided by the total PR sampled area for data during 1998–2009. In general, there are not many changes in the preference of locations of 20-dBZ echo at different altitudes. At 2 and 4 km (Figs. 10a,b), 20-dBZ echoes occur more frequently over the NWP and EPA than other basins. At 7 and 10 km (Figs. 10c,d), 20-dBZ echoes over the NWP dominate.

The 95th percentiles and median profiles of maximum radar reflectivity, 20-dBZ area, and 35-dBZ area are compared in Fig. 11 for the six basins. The maximum radar reflectivity profiles are very similar in different basins (Figs. 11a,b). No difference is seen for the near-surface reflectivity. Above the freezing level, NIO TC RPPFs reach slightly higher altitudes, while ATL TC RPPFs have slightly higher reflectivity at midlevel (8–12 km), which helps explain why ATL TCs have a higher lightning production. ATL TC RPPFs have smaller

² Some inner-core features, especially eyewalls, that are defined as MCSs in this study are different from the MCSs in outer rainbands of hurricanes or in tropical disturbances or depressions.

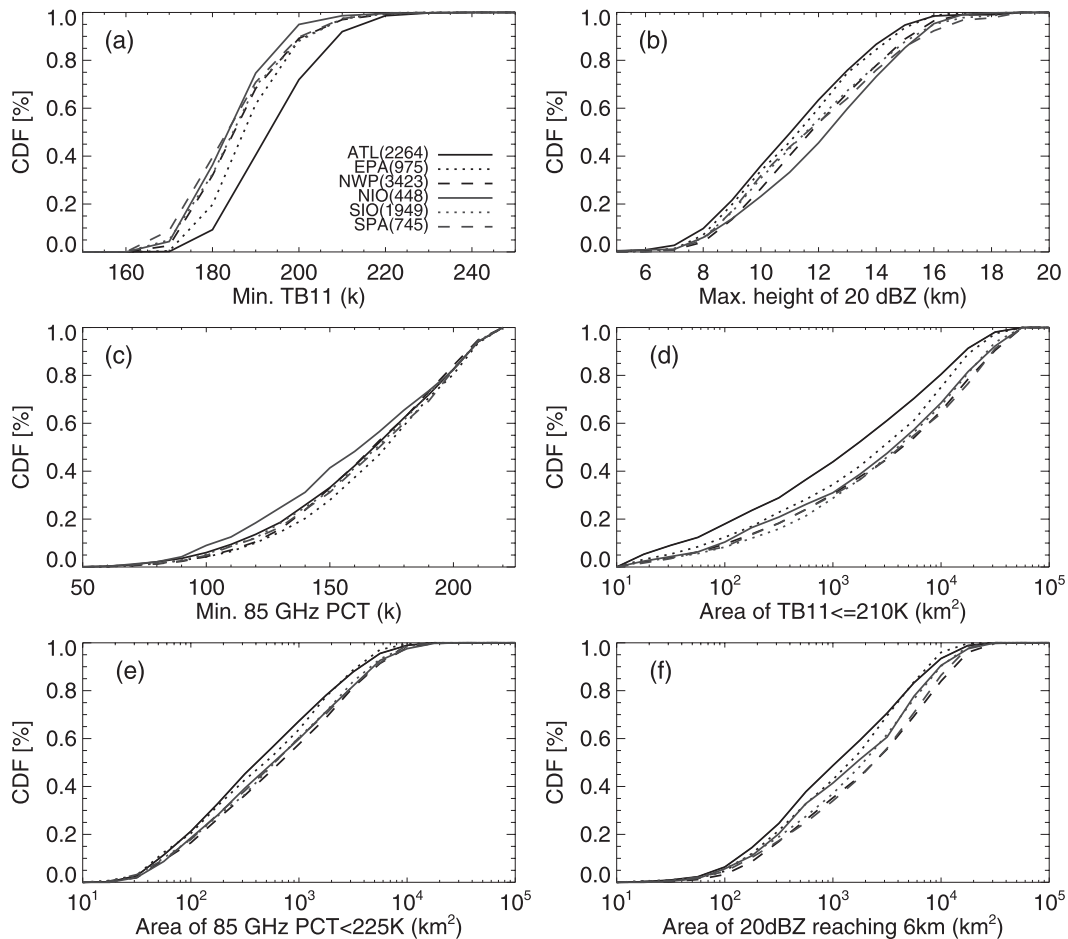


FIG. 9. Cumulative distribution functions (CDFs) of convective intensity inferred from (a) minimum T_{B11} , (b) maximum height of 20-dBZ echo, and (c) minimum 85-GHz PCT and CDFs of convective area inferred from (d) area of $T_{B11} \leq 210$ K, (e) area of minimum 85-GHz PCT < 225 K, and (f) area of 20 dBZ reaching 6 km over six basins for TC MCSs (derived from RPPFs; see text for details) from 1998 to 2009. TC MCS sample size of each basin is indicated.

20-dBZ area and reach lower altitudes than those in other basins. NWP and SPA TC RPPFs have larger 35-dBZ area than those in other basins. Overall, the differences of these profiles in different basins are rather subtle, and the similarities dominate. This result confirms the previous studies showing that convective systems over tropical oceans including TCs generally produce weaker vertical motions and have weaker convective intensity than their continental counterparts (LeMone and Zipser 1980; Lucas et al. 1994).

c. Diurnal variations of TC rainfall

Most studies of the diurnal variations of TCs used IR measurements (Browner et al. 1977; Muramatsu 1983; Steranka et al. 1984; Kossin 2002) and TC best-track winds (Cerveny and Balling 2005). By using IR data, the metrics are limited to the area covered by cirrus whose IR

cloud-top temperature is less than a certain threshold, and the average brightness temperature T_B values with a certain distance from the storm center. Browner et al. (1977) found an afternoon peak [1700 local solar time (LST)] and early morning minimum (0300 LST) for the area of cloudiness in eight Atlantic TCs by using temperature thresholds ranging from 253 to 233 K. This is similar to Steranka et al.'s (1984) result for the outer rainband regions for 23 TCs in the ATL. But for the inner-core region with very cold brightness temperatures (where deep convection exists), an early morning maximum is found by Steranka et al. (1984). On the other hand, Kossin (2002) found a semidiurnal oscillation for the ATL hurricanes by using IR cloud-top temperature measurements of 21 ATL storms in 1999. No diurnal variations of TC rainfall have been documented using satellite data. An important application of the TRMM

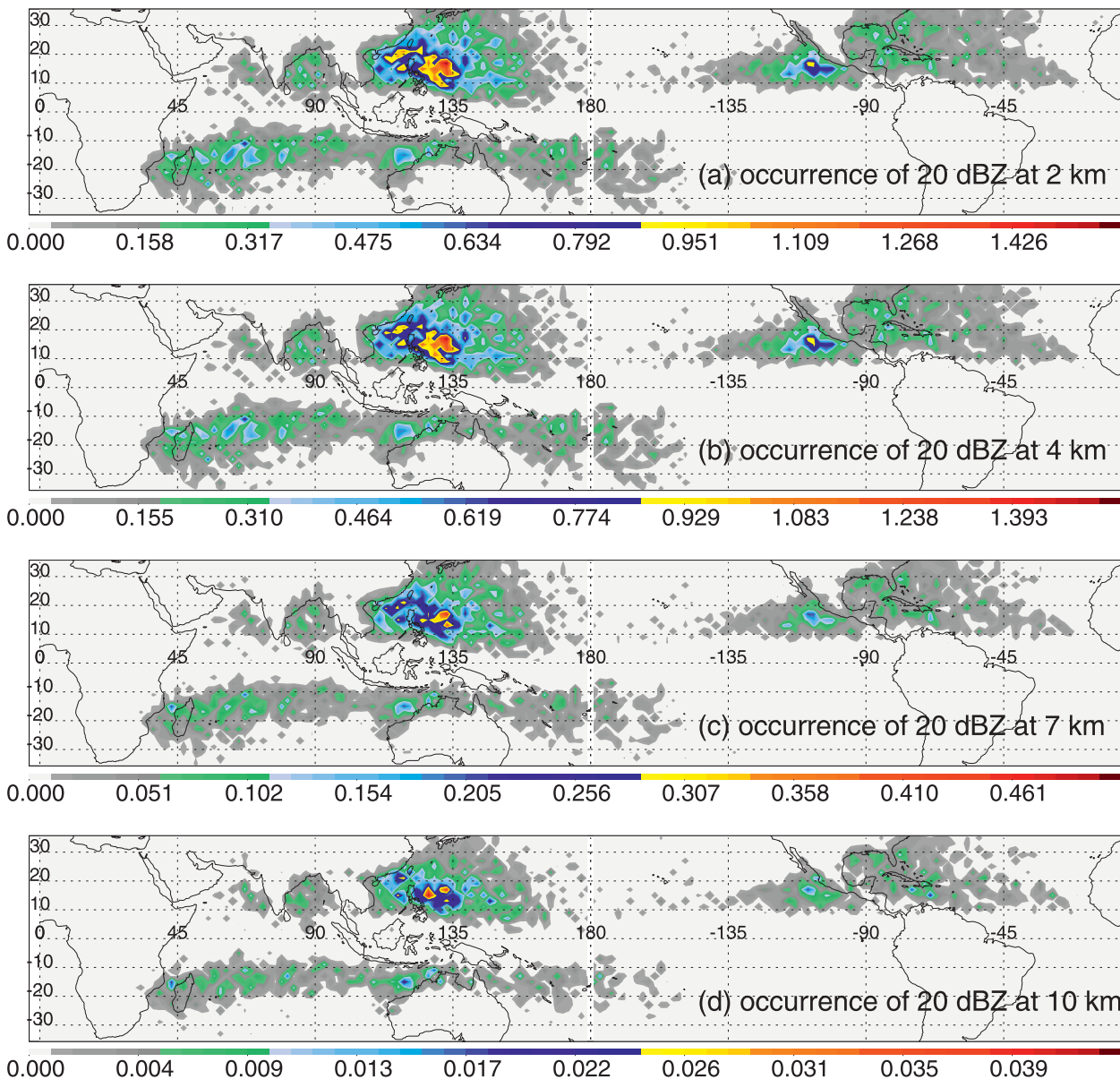


FIG. 10. Occurrence of PR reflectivity greater than 20 dBZ (%) at (a) 2, (b) 4, (c) 7, and (d) 10 km derived from TC RPPFs in 1998–2009. Note that the scales are different for (a)–(d).

TCPF database is to study the diurnal variations of TC rainfall using TRMM rainfall products. Figure 12 shows 3B42 3-hourly rainfall maps for 1998–2009 global TCs. Globally, TC rainfall peaks at 0430–0730 LST, then decreases to a minimum at 1930–2230 LST. Since rainfall is more related to deep convection than cirrus canopy area, it is expected that the phase of the TC rainfall diurnal oscillation is not consistent with Browner et al.’s (1977) results using warmer T_B thresholds. On the other hand, our result is similar to those derived from coldest IR T_B thresholds (Muramatsu 1983; Lajoie and Butterworth 1984), which are more associated with deep

convection. Table 6 presents mean values of global 3B42 TC monthly rain for different local times. We define the amplitude of the diurnal oscillation as (maximum – minimum)/mean. The global TC rainfall diurnal variation amplitude is about 20% as seen from Table 6. Similar diurnal variations are found by using PR 2A25 rainfall estimates for TCs (not shown here).

A strong land–ocean contrast is found for diurnal variations of precipitation systems (Nesbitt and Zipser 2003; Liu and Zipser 2008). To investigate the land and ocean difference for TCs, time series of 3B42 volumetric rain are compared for land and ocean in Figs. 13a,b. Consistent

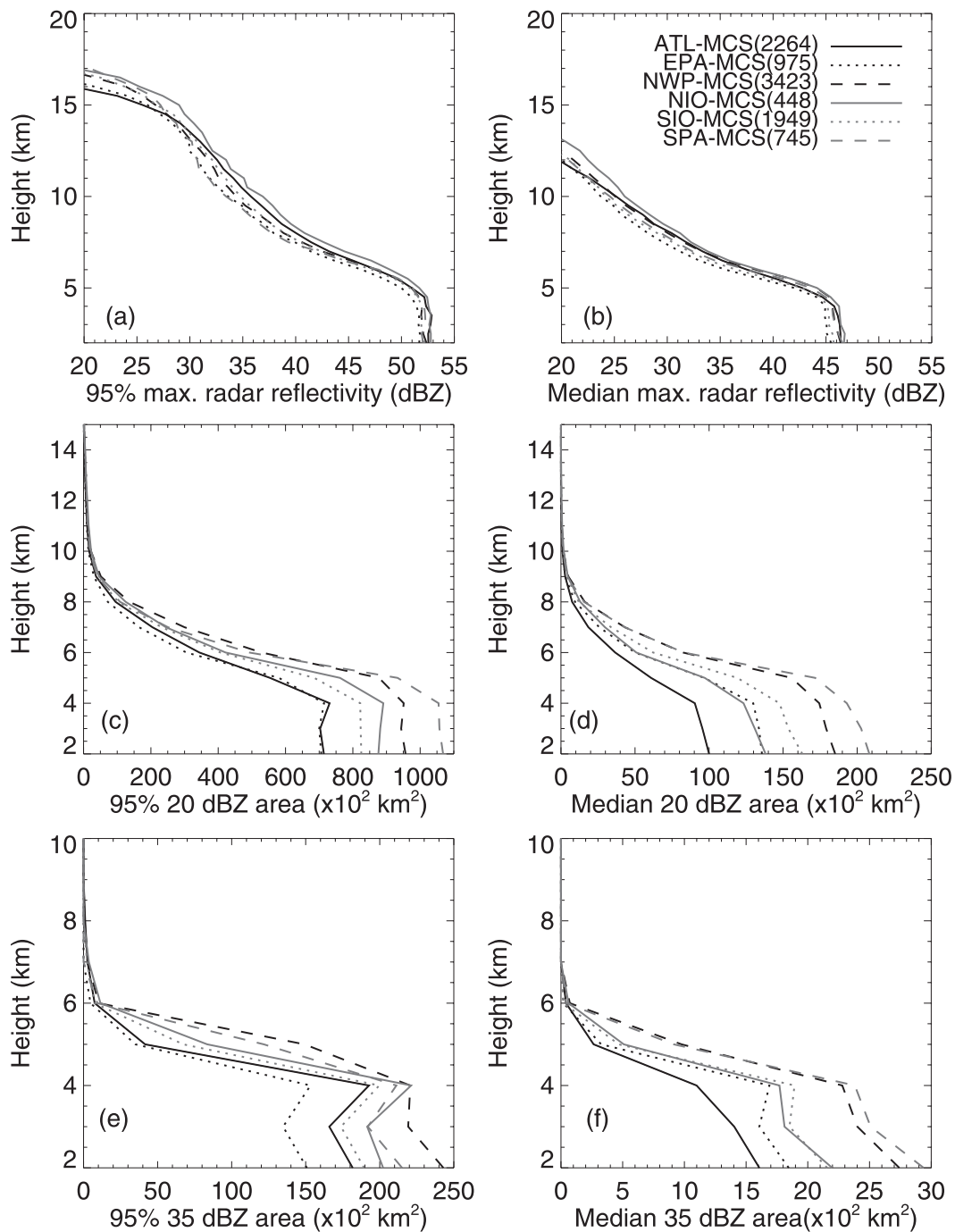


FIG. 11. The 95th percentile and median of vertical profiles of (a),(b) maximum radar reflectivity, (c),(d) 20-dBZ area, and (e),(f) 35-dBZ area of TC MCSs from 1998 to 2009 over six basins. Note that scales are different for (a)–(f).

with past studies for general tropical precipitation (Yang and Slingo 2001; Nesbitt and Zipser 2003; Liu and Zipser 2008), an early morning (0430–0730 LST; 3B42 3-hourly averaged rainfall, so 0430–0730 LST is labeled as 0600 LST in Fig. 13) peak is obvious for TC precipitation over oceans (Fig. 13a), but with less

amplitude. The minimum is at 1930–2230 LST. However, although a late afternoon maximum has been confirmed by past studies (Nesbitt and Zipser 2003; Liu and Zipser 2008) for general overland precipitation and convection systems, the TC rainfall over land has double peaks (Fig. 13b): one around 0130–0730 LST and one

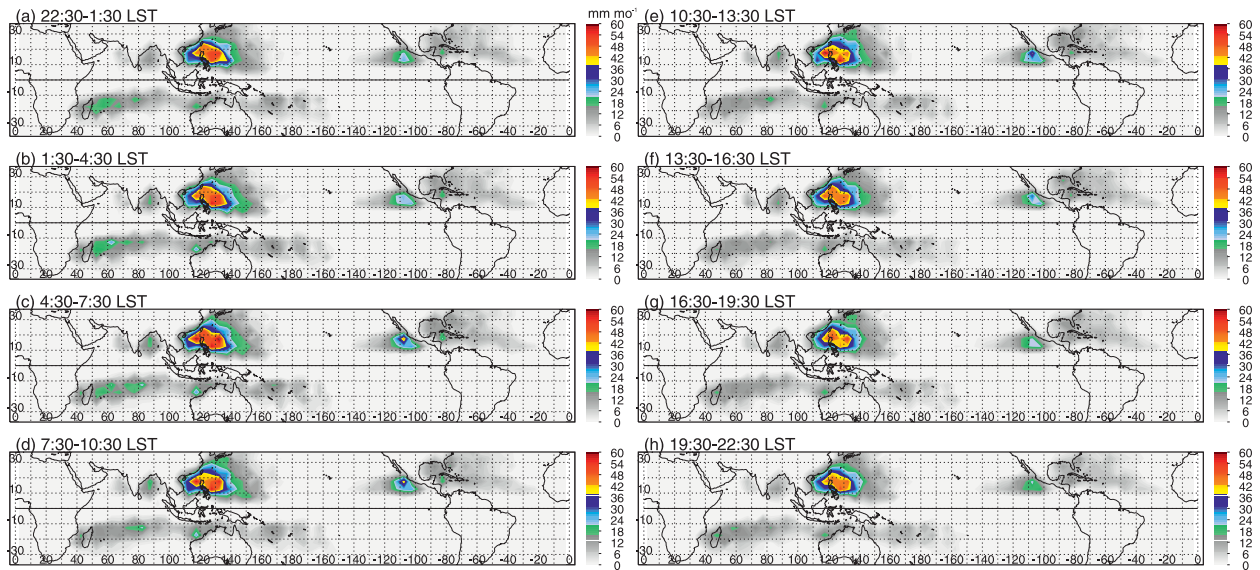


FIG. 12. The 3B42 TC monthly rain from 1998 to 2009 at (a) 2230–0130, (b) 0130–0430, (c) 0430–0730, (d) 0730–1030, (e) 1030–1330, (f) 1330–1630, (g) 1630–1930, and (h) 1930–2230 LST.

at 1630–1930 LST. The minimum is at 1030–1330 LST. The second peak can be explained by the diurnal heating of the land that enhances convection. The first peak might be associated with the oceanic characteristics of the TC systems even after making landfall.

To investigate the diurnal variation of heavy rain regions in TCs, Figs. 13c,d present the time series of TC volumetric rain for regions with rain rate greater than 5 mm h⁻¹. Over land (Fig. 13d), the phase of diurnal cycle in heavy rain regions is similar to all TC rain regions (Fig. 13b), but the amplitude (about 40%–50%) is much higher. Over oceans (Fig. 13c), the maximum is at 0430–0730 LST, but the minimum is at 1330–1630 LST. Contributions from different storm intensity categories [e.g., hurricane (HUR), tropical storm (TS), and tropical depression (TD)] are shown in different colors in Fig. 13. No big difference of diurnal variations is seen from different storm intensities.

4. Summary

This paper introduces the construction and applications of a TRMM-based TCPF database. This database is built upon the existing UU TRMM precipitation feature database. Over 1000 TCs are included for six global TC-prone basins from 1998 to 2009. TRMM measurements

of radar, visible and infrared sensors, passive microwave radiometers, and lightning sensors for TCs are collocated and integrated with TC best track and NCEP reanalysis parameters. The TRMM 3B42 rainfall product is also used to build a parallel TCPF dataset. Three levels of TRMM TCPF product are constructed following the same construction concept as in UU TRMM PF database. New convective cell feature definitions are added as a result of the recent update of the parental TRMM database.

The Web application of the database provides a search engine for users to easily find TC overpasses by TRMM, as well as download the level 1 data and best-track data and corresponding images. The Google Earth function adapted from the UU TRMM database Web application is very powerful and enable users to create cross sections of PR reflectivity for any TC TRMM orbits of interest.

Besides the Web application, three research applications of examining regional and diurnal variations of TC convection and rainfall are explored by using the TCPF database. More potential research applications of the database include, but are not limited to, 1) relationships between the storm intensity/intensity change and convective and rainfall characteristics of TCPFs; 2) comparison of 2A25, 2A12, and 3B42 rainfall retrievals for TCs; and 3) regional, seasonal, and diurnal variations of TC size, which can be defined by either rain or convective

TABLE 6. Mean values of TC 3B42 rain in Fig. 12.

| Time (LST) | 2230–0130 | 0130–0430 | 0430–0730 | 0730–1030 | 1030–1330 | 1330–1630 | 1630–1930 | 1930–2230 |
|--|-----------|-----------|-----------|-----------|-----------|-----------|-----------|-----------|
| Mean TC monthly rain (mm month ⁻¹) | 2.07 | 2.24 | 2.34 | 2.21 | 2.09 | 2.06 | 2.01 | 2.97 |

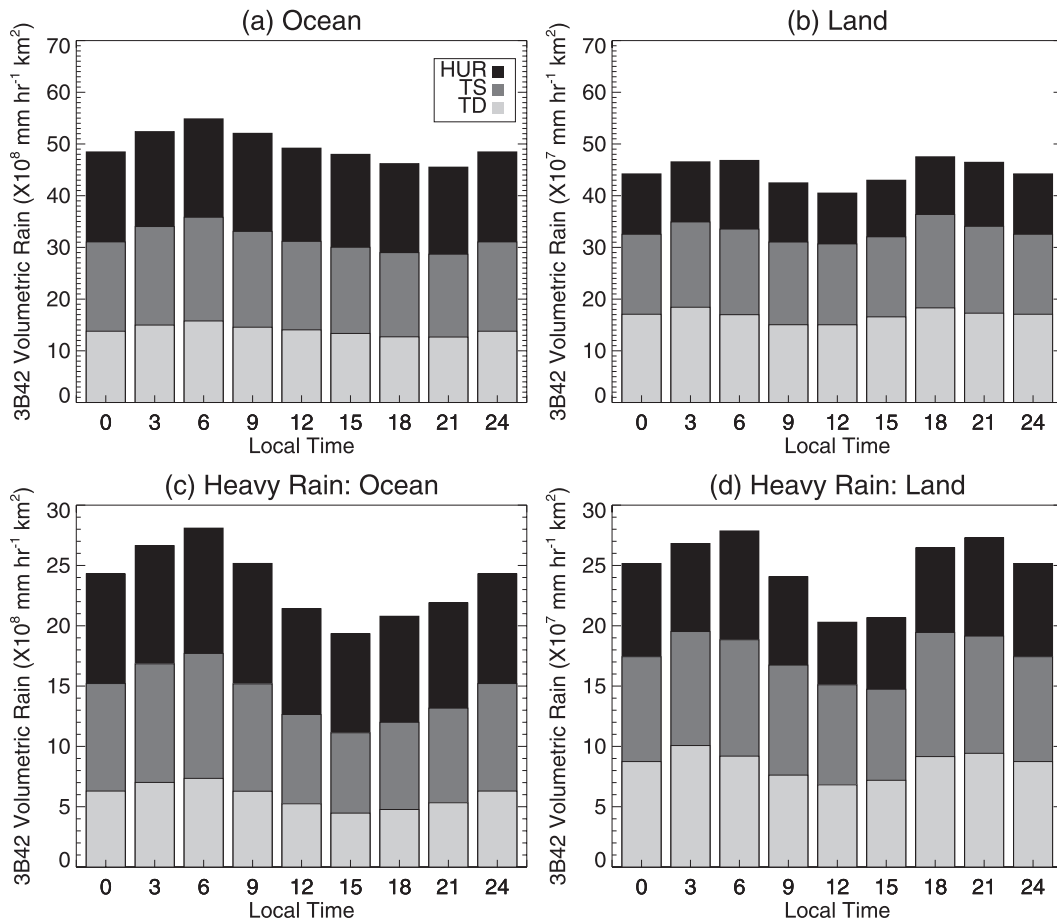


FIG. 13. Diurnal variations of volumetric rain for all 3B42 TCPFs over (a) ocean and (b) land, and for heavy rain regions only in 3B42 TCPFs over (c) ocean and (d) land from 1998 to 2009. Volumetric rains from different storm intensity categories (e.g., HUR, TS, and TD) are shown in different shades.

parameters provided in the database. Future work includes separating TCPFs into eyewall, inner-band, and outer-band regions, which will allow research applications involving different TC regions. It is also a future work direction to add Quick Scatterometer (QuikSCAT) sea surface wind and TMI and SSM/I sea surface temperature data into the database.

Acknowledgments. Support for this study is provided by the NASA Precipitation Measurement Mission (PMM) Grant NNX07AL41G/NNX10AE28G, NASA New Investigator Program (NIP) Grant NNX08AT20G/NNX10AG55G, and NASA Hurricane Science Research Program (HSRP) Grant NNX09AC42G/NNX10AG34G. The authors thank Ramesh Kakar and Ming-Ying Wei (NASA headquarters) for their continued support of TRMM/PMM and hurricane sciences. Discussions with Dan Cecil at UAH and John Molinari at the University at Albany were very helpful. We also give our

acknowledgments to Deanna Hense and two other anonymous reviewers for their helpful comments. Ellen Ramirez helped on identifying landfalling TCs from 1998 to 2004. Michael Peterson has been very helpful on adapting the Google Earth Web feature to the TCPF database.

REFERENCES

- Awaka, J., T. Iguchi, and K. Okamoto, 1998: Early results on rain type classification by the Tropical Rainfall Measuring Mission (TRMM) precipitation radar. *Proc. Eighth URSI Commission F Triennial Open Symp.*, Aveiro, Portugal, International Union of Radio Science, 143–146.
- Black, R. A., and J. Hallett, 1986: Observations of the distribution of ice in hurricanes. *J. Atmos. Sci.*, **43**, 802–822.
- , and —, 1999: Electrification of the hurricane. *J. Atmos. Sci.*, **56**, 2004–2028.
- Boccippio, D. J., W. J. Koshak, and R. J. Blakeslee, 2002: Performance assessment of the optical transient detector and lightning imaging sensor. Part I: Predicted diurnal variability. *J. Atmos. Oceanic Technol.*, **19**, 1318–1332.

- Bosart, L. F., C. S. Velden, W. E. Bracken, J. Molinari, and P. G. Black, 2000: Environmental influences on the rapid intensification of Hurricane Opal (1995) over the Gulf of Mexico. *Mon. Wea. Rev.*, **128**, 322–352.
- Browner, S. P., W. L. Woodley, and C. G. Griffith, 1977: Diurnal oscillation of the area of cloudiness associated with tropical storms. *Mon. Wea. Rev.*, **105**, 856–864.
- Cecil, D. J., and E. J. Zipser, 1999: Relationships between tropical cyclone intensity and satellite-based indicators of inner core convection: 85-GHz ice-scattering signature and lightning. *Mon. Wea. Rev.*, **127**, 103–123.
- , and —, 2002: Reflectivity, ice scattering, and lightning characteristics of hurricane eyewalls and rainbands. Part II: Intercomparison of observations. *Mon. Wea. Rev.*, **130**, 785–801.
- , —, and S. W. Nesbitt, 2002: Reflectivity, ice scattering, and lightning characteristics of hurricane eyewalls and rainbands. Part I: Quantitative description. *Mon. Wea. Rev.*, **130**, 769–784.
- Cerveny, R. S., and R. C. Balling Jr., 2005: Variations in the diurnal character of tropical cyclone wind speeds. *Geophys. Res. Lett.*, **32**, L06706, doi:10.1029/2004GL021177.
- Douglas, A. V., and P. J. Englehart, 2001: The role of eastern North Pacific tropical storms in the rainfall climatology of western Mexico. *Int. J. Climatol.*, **21**, 1357–1370.
- Gottelman, A., M. L. Salby, and F. Sassi, 2002: The distribution and influence of convection in the tropical tropopause region. *J. Geophys. Res.*, **107**, 4080, doi:10.1029/2001JD001048.
- Gray, W. M., 1968: Global view of the origin of tropical disturbances and storms. *Mon. Wea. Rev.*, **96**, 669–700.
- Huffman, G. J., and Coauthors, 2007: The TRMM Multisatellite Precipitation Analysis (TMPA): Quasi-global, multiyear, combined-sensor precipitation estimates at fine scales. *J. Hydrometeorol.*, **8**, 38–55.
- Iguchi, T., T. Kozu, R. Meneghini, J. Awaka, and K. Okamoto, 2000: Rain-profiling algorithm for the TRMM precipitation radar. *J. Appl. Meteor.*, **39**, 2038–2052.
- Jiang, H., and E. J. Zipser, 2010: Contribution of tropical cyclones to the global precipitation from eight seasons of TRMM data: Regional, seasonal, and interannual variations. *J. Climate*, **23**, 1526–1543.
- Kaplan, J., and M. DeMaria, 2003: Large-scale characteristics of rapidly intensifying tropical cyclones in the North Atlantic basin. *Wea. Forecasting*, **18**, 1093–1108.
- Kelley, O. A., J. Stout, and J. B. Halverson, 2004: Tall precipitation cells in tropical cyclones eyewalls are associated with tropical cyclone intensification. *Geophys. Res. Lett.*, **31**, L24112, doi:10.1029/2004GL021616.
- , —, and —, 2005: Hurricane intensification detected by continuously monitoring tall precipitation in the eyewall. *Geophys. Res. Lett.*, **32**, L20819, doi:10.1029/2005GL023583.
- Kerns, B., and E. Zipser, 2009: Four years of tropical ERA-40 vorticity maxima tracks. Part II: Differences between developing and nondeveloping disturbances. *Mon. Wea. Rev.*, **137**, 2576–2591.
- Kossin, J. P., 2002: Daily hurricane variability inferred from GOES infrared imagery. *Mon. Wea. Rev.*, **130**, 2260–2270.
- Kummerow, C., W. S. Olson, and L. Giglio, 1996: A simplified scheme for obtaining precipitation and vertical hydrometeor profiles from passive microwave sensors. *IEEE Trans. Geosci. Remote Sens.*, **34**, 1213–1232.
- , W. Barnes, T. Kozu, J. Shiue, and J. Simpson, 1998: The Tropical Rainfall Measuring Mission (TRMM) sensor package. *J. Atmos. Oceanic Technol.*, **15**, 809–817.
- , and Coauthors, 2001: The evolution of the Goddard profiling algorithm (GPROF) for rainfall estimation from passive microwave sensors. *J. Appl. Meteor.*, **40**, 1801–1820.
- Laing, A. G., and J. M. Fritsch, 1997: The global population of mesoscale convective complexes. *Quart. J. Roy. Meteor. Soc.*, **123**, 389–405.
- Lajoie, F. A., and I. J. Butterworth, 1984: Oscillation of high-level cirrus and heavy precipitation around Australian region tropical cyclones. *Mon. Wea. Rev.*, **112**, 535–544.
- Landsea, C. W., and Coauthors, 2004: The Atlantic hurricane database reanalysis project: Documentation for the 1851–1910 alterations and additions to the HURDAT database. *Hurricanes and Typhoons: Past, Present, and Future*, R. J. Murnane and K.-B. Liu, Eds., Columbia University Press, 177–221.
- , and Coauthors, 2008: A reanalysis of the 1911–20 Atlantic hurricane database. *J. Climate*, **21**, 2138–2168.
- Larson, J., Y. Zhou, and R. W. Higgins, 2005: Characteristics of landfalling tropical cyclones in the United States and Mexico: Climatology and interannual variability. *J. Climate*, **18**, 1247–1262.
- LeMone, M. A., and E. J. Zipser, 1980: Cumulonimbus vertical velocity events in GATE. Part I: Diameter intensity and mass flux. *J. Atmos. Sci.*, **37**, 2444–2457.
- Liu, C., cited 2007: University of Utah TRMM precipitation and cloud feature database description, v1.0. [Available online at http://trmm.chpc.utah.edu/docs/trmm_database_description_v1.0.pdf.]
- , and E. J. Zipser, 2005: Global distribution of convection penetrating the tropical tropopause. *J. Geophys. Res.*, **110**, D23104, doi:10.1029/2005JD006063.
- , and —, 2008: Diurnal cycles of precipitation, clouds, and lightning in the tropics from 9 years of TRMM observations. *Geophys. Res. Lett.*, **35**, L04819, doi:10.1029/2007GL032437.
- , —, and S. W. Nesbitt, 2007: Global distribution of tropical deep convection: Different perspectives from TRMM infrared and radar data. *J. Climate*, **20**, 489–503.
- , —, D. J. Cecil, S. W. Nesbitt, and S. Sherwood, 2008: A cloud and precipitation feature database from 9 years of TRMM observations. *J. Appl. Meteor. Climatol.*, **47**, 2712–2728.
- Lonfat, M., F. D. Marks, and S. S. Chen, 2004: Precipitation distribution in tropical cyclones using the Tropical Rainfall Measuring Mission (TRMM) Microwave Imager: A global perspective. *Mon. Wea. Rev.*, **132**, 1645–1660.
- , R. Rogers, T. Marchok, and F. D. Marks, 2007: A parametric model for predicting hurricane rainfall. *Mon. Wea. Rev.*, **135**, 3086–3097.
- Lucas, C., E. J. Zipser, and M. A. LeMone, 1994: Vertical velocity in oceanic convection off tropical Australia. *J. Atmos. Sci.*, **51**, 3183–3193.
- Mapes, B. E., and R. A. Houze, 1993: Cloud clusters and superclusters over the oceanic warm pool. *Mon. Wea. Rev.*, **121**, 1398–1416.
- Mohr, K. I., and E. J. Zipser, 1996: Defining mesoscale convective systems by their 85-GHz ice-scattering signatures. *Bull. Amer. Meteor. Soc.*, **77**, 1179–1189.
- Muramatsu, T., 1983: Diurnal variations of satellite-measured T_{BB} areal distribution and eye diameter of mature typhoons. *J. Meteor. Soc. Japan*, **61**, 77–90.
- Nesbitt, S. W., and E. J. Zipser, 2003: The diurnal cycle of rainfall and convective intensity according to three years of TRMM measurements. *J. Climate*, **16**, 1456–1475.

- , —, and D. J. Cecil, 2000: A census of precipitation features in the tropics using TRMM: Radar, ice scattering, and lightning observations. *J. Climate*, **13**, 4087–4106.
- , R. Cifelli, and S. A. Rutledge, 2006: Storm morphology and rainfall characteristics of TRMM precipitation features. *Mon. Wea. Rev.*, **134**, 2702–2721.
- Orville, R. E., and R. W. Henderson, 1986: Global distribution of midnight lightning: September 1977 to August 1978. *Mon. Wea. Rev.*, **114**, 2640–2653.
- Petersen, W. A., and S. A. Rutledge, 2001: Regional variability in tropical convection: Observations from TRMM. *J. Climate*, **14**, 3566–3586.
- Rappaport, E. N., 2000: Loss of life in the United States associated with recent Atlantic tropical cyclones. *Bull. Amer. Meteor. Soc.*, **81**, 2065–2074.
- Shay, L. K., G. J. Goni, and P. G. Black, 2000: Effects of a warm oceanic feature on Hurricane Opal. *Mon. Wea. Rev.*, **128**, 1366–1383.
- Simpson, J., J. B. Halverson, B. S. Ferrier, W. A. Peterson, R. H. Simpson, R. Blakeslee, and S. L. Durden, 1998: On the role of “hot towers” in tropical cyclone formation. *Meteor. Atmos. Phys.*, **67**, 15–35.
- Spencer, R. W., H. G. Goodman, and R. E. Hood, 1989: Precipitation retrieval over land and ocean with the SSM/I: Identification and characteristics of the scattering signal. *J. Atmos. Oceanic Technol.*, **6**, 254–273.
- Steiner, M., R. A. Houze Jr., and S. Yuter, 1995: Climatological characterization of three-dimension storm structure from operational radar and rain gauge data. *J. Appl. Meteor.*, **34**, 1978–2007.
- Steranka, J., E. B. Rodgers, and R. C. Gentry, 1984: The diurnal variation of Atlantic Ocean tropical cyclone cloud distribution inferred from geostationary satellite infrared measurements. *Mon. Wea. Rev.*, **112**, 2338–2344.
- , —, and —, 1986: The relationship between satellite measured convective bursts and tropical cyclone intensification. *Mon. Wea. Rev.*, **114**, 1539–1546.
- Takahashi, T., 1978: Riming electrification as a charge generation mechanism in thunderstorms. *J. Atmos. Sci.*, **35**, 1536–1548.
- Tuleya, R. E., M. DeMaria, and R. J. Kuligowski, 2007: Evaluation of GFDL and simple statistical model rainfall forecasts for U.S. landfalling tropical storms. *Wea. Forecasting*, **22**, 56–70.
- Weng, F., L. Zhao, R. Ferraro, G. Poe, X. Li, and N. Grody, 2003: Advanced Microwave Sounding Unit cloud and precipitation algorithms. *Radio Sci.*, **38**, 8068–8079.
- Xu, W., E. J. Zipser, C. Liu, and H. Jiang, 2010: On the relationships between lightning frequency and thundercloud parameters of regional precipitation systems. *J. Geophys. Res.*, **115**, D12203, doi:10.1029/2009JD013385.
- Yang, G.-Y., and J. Slingo, 2001: The diurnal cycle in the tropics. *Mon. Wea. Rev.*, **129**, 784–801.
- Zhao, L., and F. Weng, 2002: Retrieval of ice cloud parameters using the Advanced Microwave Sounding Unit. *J. Appl. Meteor.*, **41**, 384–395.
- Zipser, E. J., 1994: Deep cumulonimbus cloud systems in the tropics with and without lightning. *Mon. Wea. Rev.*, **122**, 1837–1851.
- , D. Cecil, C. Liu, S. Nesbitt, and D. Yorty, 2006: Where are the most intense thunderstorms on earth? *Bull. Amer. Meteor. Soc.*, **87**, 1057–1071.